





Intrinsic equilibrium of stably autorotating samarasPeixing Niu ^{1,2} Michael D. Atkins,³ Yanyan Liu,^{1,2} Moxiao Li ^{1,2} Tian Jian Lu ^{1,2,4} and Tongbeum Kim ^{1,2,3,4}¹*State Key Laboratory of Mechanics and Control of Mechanical Structures, Nanjing University of Aeronautics and Astronautics, Nanjing 210016, China*²*MIT Key Laboratory of Multifunctional Lightweight Materials and Structures, Nanjing University of Aeronautics and Astronautics, Nanjing 210016, China*³*School of Mechanical, Industrial and Aeronautical Engineering, University of the Witwatersrand, Johannesburg 2000, South Africa*⁴*State Key Laboratory for Strength and Vibration of Mechanical Structures, Xi'an Jiaotong University, Xi'an 710049, China*

(Received 15 March 2022; accepted 29 June 2022; published 26 July 2022)

During descent, a single-winged maple seed (samara) can naturally reach a delicate equilibrium state, stable autorotation, before landing. This article reveals the intrinsic equilibrium of a particular type of samaras in terms of measurable aerodynamic and geometric parameters. To this end, we conducted a series of *in situ* measurements for the rate of vertical descent (exclusive of crosswind) of an autorotating samara in a natural range of samara sizes and masses. We then extended the range of size and mass by introducing artificial samaras, with discrete mass elements purposely designed to approximate the asymmetrical and nonuniform distribution of mass found with natural samaras. Based on the widened range, a fundamental *nondimensional* correlation of dynamic pressure and disc loading was generalized, where all stable autorotation descent profiles collapse to a single descent characteristic curve, irrespective of the size and mass of the natural and artificial samara's specimens. Results reveal that for stably autorotating (both natural and artificial) samaras, their terminal descent velocity (expressed as dynamic pressure) and disc loading attained equilibrium at a value that is inversely proportional to the coefficient of lift.

DOI: [10.1103/PhysRevE.106.014405](https://doi.org/10.1103/PhysRevE.106.014405)**I. INTRODUCTION**

Samaras are single-winged fruits and seeds (e.g., maple seeds) that exhibit interesting flight behavior when falling from their parent tree (the common H is ~ 2.5 m). On the way down towards the ground, samaras were observed to complete three distinct stages [1–4] of falling as shown in Fig. 1. In particular, the seed initially is in *free fall* when released from the tree, followed by *transient positioning*, and finally establishing *stable autorotation*. The period of each stage depends on the initial attitude of the samara when it breaks free from the tree [1]. Once stable autorotation is reached, the lift force of the samara is in equilibrium with its gravitational force, leading to the so-called “terminal” descent velocity [5–10]. This unique aerodynamic behavior of the samaras during dispersal, thus has inspired studies in biomimetics [11–17]. Here the common aim is to devise a small lightweight flying object that can prolong its flight/floating time without additional power input and moving parts [17]. To realize these designs, a grasp of the physical mechanisms underpinning stably autorotating single-winged bodies, e.g., samaras, are required.

Despite the multitude of previous studies focusing on various aspects of the descending autorotating single-winged body (e.g., samara), understanding the natural mechanisms governing stable autorotation remains elusive. Previous studies have identified that, during stable autorotation, the lift generated by a single-winged body is enhanced by the development of leading-edge vortices [18–20], thus sustaining

stable autorotation at the delicate equilibrium conditions [21,22]. It is believed that nature has evolved the descent dynamics of the samara to shorten the free falling and transient positioning periods and prolong the stable autorotation period via “intrinsic equilibrium.” Consequently, the dispersal period and range of the seed are significantly extended [2]. However, the present knowledge gained on the equilibrium of forces and moments that sustain the stable autorotation is largely qualitative and implicit. To address this issue, this article unveils the existence of an intrinsic equilibrium reached in a particular type of samaras (*Acer buergerianum*) and demonstrates the generalization of the flight characteristics of the samaras based on measured aerodynamic and geometric parameters.

II. DESCENT KINEMATICS

This section provides the descent kinematics of natural and artificial samara whose descent in the quiescent air shows the intrinsic equilibrium and the generalization of the stable autorotation.

A. Natural samara

We measured the velocity of the samara when falling, using an experimental setup consisting of a high-speed camera that enabled 50 *in situ* instantaneous velocity data points to be obtained while the winged seed was released by an automatic releasing device and thus descent, as shown in Fig. S1

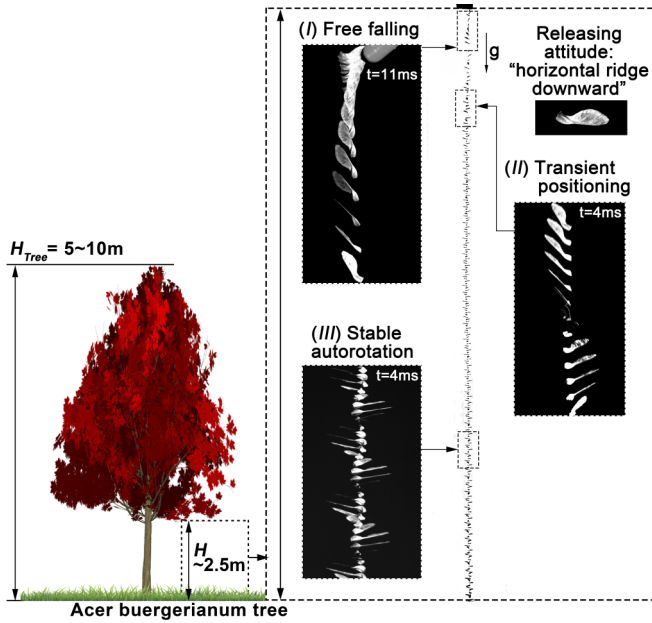


FIG. 1. Typical trajectory of a descending samara (*Acer buergerianum*) in the absence of crosswind (presently captured by a highspeed camera, for the sake of clarity, time interval t of trajectories is different), showing *Stage I*: free falling, *Stage II*: transient positioning, and *Stage III*: stable autorotation before landing, consistent with previous studies [1–4] where the initial attitude is “horizontal ridge (or leading-edge) downward.”

(Supplemental Material [23], which include Refs. [24,25]). With the aid of the panorama of *in situ* velocity measurements (in absence of crosswind), this article experimentally reveals three distinct stages of a vertically descending samara from release to landing: *Stage I*: free falling, *Stage II*: transient positioning (featured by diminishing oscillatory pitching [2]), and *Stage III*: stable autorotation (with trivial oscillatory pitching [2]) before landing, in contrast to previous classification via qualitative visualized images [1,3] and numerical simulations [2]. Figure 2(a) displayed the instantaneous velocities obtained for four selected natural samara specimens with the mass varying from 14.0 to 50.0 mg (#1–4, Table I [23]). Correspondingly, the terminal descent velocity increases proportionally with natural samara mass, from 0.65 m/s to 1.2 m/s. However, despite each samara attaining a distinct terminal velocity in accordance with its mass, the descent velocity profiles of each samara specimen share common characteristics with respect to the above three stages.

In particular, at *Stage III*: stable autorotation (Supplemental Video 1 [23]), the pitch and cone angles of each tested samara remain largely unchanged as the specimen descends (Figs. S2 and S3 [23]), each reaching a terminal velocity well before landing. The common altitudinal variation of descent velocities in Fig. 2(a) implies that an intrinsic equilibrium is reached in stably autorotating samaras, regardless of their masses and subtly different wing shapes.

To establish a key parameter that links pivotal constituents dictating such stable autorotation, we adopted the linear momentum theorem to analyze the single-winged body as an idealized actuator disc that was assumed to be configured by

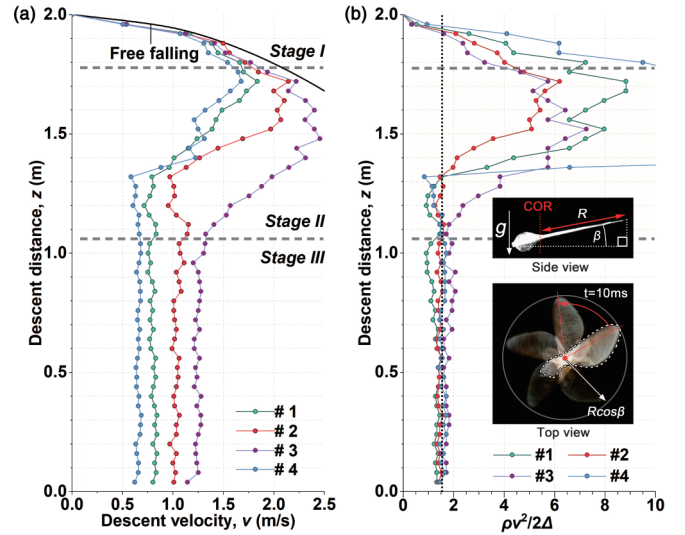


FIG. 2. Descent of natural samaras (*Acer buergerianum*) in absence of crosswind. (a) Measurement data showing *Stage I*: free falling, *Stage II*: transient positioning, and *Stage III*: stable autorotation before landing. (b) Generalized descent of natural samaras via Eq. (1) where the insets display a side view of the center of rotation (COR) and cone angle (β) and a top view exposed to strobe light at 100 Hz configuring an actuator disc for (Natural) Samara #1.

a stably autorotating samara, as illustrated by the inset of Fig. 2(b). During stable autorotation, the drag acts together with the lift force to establish a constant descent velocity, for these forces are in equilibrium with the total weight of the actuator disc. Following the derivation by Norberg [26], it can be shown that the dynamic pressure acting on a descending samara is scaled with the disc loading (gravitational force per unit area of actuator disc, denoted herein as Δ).

In all previous analyses, the vast data sets for descent velocity (v) as a function of disc (Δ) (or wing) loading have been commonly correlated as $v \sim \Delta$ (or $\Delta^{1/2}$), indicating their linear proportionality [5,26]. However, these *dimensional* correlations appear to conceal the general descent characteristics of samaras. Furthermore, the physical implication of the intrinsic equilibrium in a stably autorotating samara can be more clearly observed with a *dimensionless* constant to reveal the general descent characteristics of the samaras irrespective of the specimen’s mass and size. To this end, we present the descent velocity in the form of dynamic pressure ($\rho v^2/2$) normalized by the corresponding disc loading, i.e., $\rho v^2/(2\Delta)$. Then, the force equilibrium can be presented as

$$\frac{\rho v^2/2}{\Delta} = \frac{1}{C_L}, \quad (1)$$

$$\Delta = \frac{gm}{\pi R^2 \cos^2(\beta)}, \quad (2)$$

where ρ is the density of air, v is the stable descent velocity, g is the gravitational acceleration, m is the total mass, $R \cos(\beta)$ is the radius of rotation, β is the cone angle, and C_L is the lift coefficient of the actuator disc. The schematic of actuator disc is shown in Fig. S4 [23]. The lift coefficient is a collective term that depends on the angle of attack (α) along the span, pitch

angle (θ), cone angle (β), local tangential velocity ($r\omega$), and descent velocity (v), i.e., $C_L = f(\alpha, \theta, \beta, \alpha(r), r\omega, v)$, r being the spanwise coordinate. The corresponding disc loading was determined by measuring the cone angle and radius of rotation during stable floating using a vertical wind-tunnel setup. Here, an upwards air flow with a velocity that was matched to the stable descent velocity of the samara, was generated in a vertical test section that mimics the stable autorotation observed during the single wing body's descent.

The variation of descent velocity in Fig. 2(a) is then extracted to calculate the dimensionless value of $\rho v^2/(2\Delta)$ for each samara specimen, with the disc loading (Δ) independently calculated using kinematic data (i.e., R and β from superimposed images and samara mass, which is presented in Table I [23]). As shown in Fig. 2(b), the variation of $\rho v^2/(2\Delta)$ with descent distance z (measured from the release position of $H = 2.0$ m) reveals that the dynamic pressure of a descending samara can be generalized by disc loading. More importantly, the generalized value, i.e., $\rho v^2/(2\Delta)$, or the inverse of the collective lift coefficient, i.e., $1/C_L$ in Eq. (1), appears to approach *asymptotically* to a single value. In other words, for the tested natural samara specimens, the values of $\rho v^2/(2\Delta)$ collapse to a singular line during stable autorotation, irrespective of the natural samara *mass* and *size*, qualitatively consistent with the dimensional correlations [5,26].

The described measurements encompassed a natural range of samaras in terms of mass and wing geometry (wingspan). However, to affirm the *asymptotic* value between dynamic pressure and specimen disc loading during stable autorotation, a broader range of specimens is required. The difficulty we encountered is that, while natural specimens vary from seed to seed, the available masses and wingspans fall within a narrow range, thus restricting further analysis. To broaden the range, artificial single-winged bodies, termed “artificial samaras” hereafter that are capable of mimicking the descent kinematics of natural samaras, both qualitatively and quantitatively are needed. To this end, it was essential to identify key factors underpinning the stable autorotation of natural samaras.

B. Artificial samara

In line with previous studies [3,4,21,22,26,27], we hypothesized that the asymmetry of mass distribution in the natural samara is a key factor governing its stable autorotation. To obtain a more general spectrum of mass distribution, 12 additional natural samara specimens (*Acer buergerianum*) were measured. The distribution of samara mass is predominantly made up of the nut (W_1), the ridge (W_2), and the wing (W_3) (Nomenclature in Table I [23]). With denser structures located in the nut and ridge, the samara mass is distributed towards the leading edge of the wing. The total mass of a samara varies from $W_t = 14.2$ mg to 50.0 mg (Fig. S5(a) [23]), but the proportions of its three basic parts are similar, $W_1/W_t = 0.82\sim 0.91$ for the nut, $W_2/W_t = 0.06\sim 0.11$ for the ridge, and $W_3/W_t = 0.12\sim 0.20$ for the wing (Fig. S5(b) [23]). Thus, based on mass similarity using the least number of mass elements, the 18 artificial samaras are constructed with three discrete mass elements (W_1 , W_2 , and W_3) with natural mass proportions to approximate the asymmetrical, nonuniform,

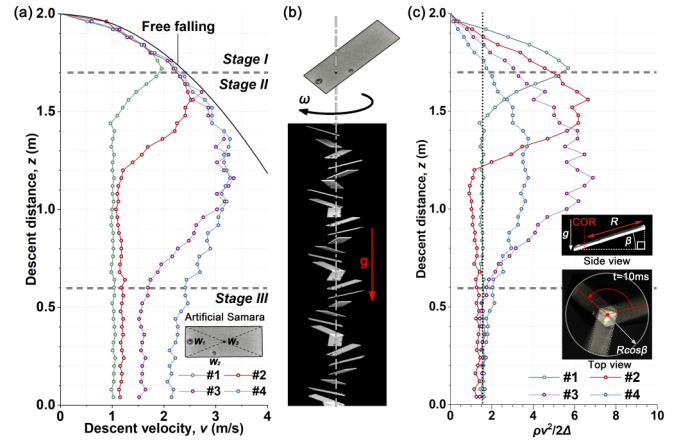


FIG. 3. Descent of artificial samaras without crosswind. (a) Measurement data showing *Stage I*: free falling, *Stage II*: transient positioning, and *Stage III*: stable autorotation before landing. (b) A superimposed image of stably autorotating artificial Samara #1. (c) Generalized descent of artificial samaras via Eq. (1) where the insets display a side view of a cone angle (β) and a top view exposed to strobe light at 100 Hz configuring an actuator disc for artificial Samara #1.

and continuous variation of mass found with natural samaras (Nomenclature in Table II [23]).

Specifically, built upon these mass proportions, the nut (W_1) and the ridge (W_2) were both simulated by metallic balls with varying mass. Further, to facilitate fundamental analysis of stable autorotation, the geometry of the single-winged structure is simulated using a rectangle polystyrene board, rather than a complex “samara shape.” The aspect ratio (span-to-chord, a/b) of the wing loosely mimics that of samara; the location of W_1 was roughly coincident with the midchord, while that of W_2 varied as 17.5~37.5% of the span (Table II [23]).

Instantaneous velocities of four selected artificial samaras in Fig. 3(a) depict that, upon releasing from an altitude of 2.0 m, they descend in a similar manner to natural samaras, consistently mimicking *Stage I*: free falling and *Stage III*: stable autorotation via *Stage II*: transient positioning. The stable descent velocities are nonetheless higher than those of samaras [also released from 2.0 m; Fig. 2(a)], ranging from 1.0 m/s to 2.16 m/s *as intended*: the total mass of the artificial samaras varies substantially from 40.0 to 490.0 mg (Table II [23]), relative to the range of 14.0 to 50.0 mg found for natural samaras (Fig. S5(a) [23]). The artificial samaras with smaller wingspan descend faster, but still reach the stage of stable autorotation (Supplemental Video 2 [23]). Similar to the case of natural samaras (Fig. 1), with crosswind excluded, the superimposed image of Fig. 3(b) visualizes the vertical stable descent of an artificial samara with respect to its axis of autorotation. In summary, both natural and artificial samaras with similar asymmetrical mass distribution descend in a similar manner, thus validating our hypothesis.

Analogous to natural samaras, the variation of descent velocity recalculated for each artificial samara in the dimensionless form of $\rho v^2/(2\Delta)$ in Fig. 3(c) reveals that its dynamic pressure could be generalized by the corresponding

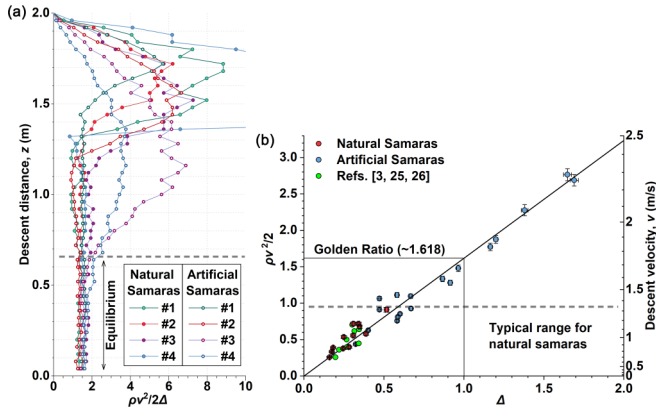


FIG. 4. Generalized descent of both natural and artificial samaras. (a) The dimensionless ratio [Eq. (1)] of both specimen types approaches a similar asymptotic value. (b) Intrinsic equilibrium in stably autorotating single-winged bodies showing a linear correlation between dynamic pressure and disc loading, with a slope that approximates the 1.618 (Golden ratio).

disc loading. Again, the generalized value, $\rho v^2 / (2\Delta)$ approaches *asymptotically* to a single value and the inherent descent characteristics of the artificial samaras are revealed since the defined dimensionless ratio for all the specimens collapse the measurement data onto a single stable autorotation curve.

III. INTRINSIC EQUILIBRIUM

Comparing the natural samaras [Fig. 2(b)] with the artificial samaras [Fig. 3(c)] demonstrates that, during the free falling and transient positioning stages, the dynamic pressure is substantially higher than disc loading, because of the significantly lower lift coefficient generated by descending single-winged bodies, inclusive of both natural and artificial samaras. However, stable autorotation, once reached, generates the lift in a way that the dynamic pressure becomes balanced by disc loading via a factor of $1/C_L$, which is constant for all the tested natural and artificial specimens.

Given that the tested natural and artificial samaras exhibit similar asymptotic value of $\rho v^2 / (2\Delta)$ [Fig. 4(a)], a linear proportionality appears to develop in *Stage III*, as $\rho v^2 / (2\Delta) = 1/C_L$. It is interesting that this *constant of proportionality* approximates a value of 1.618 (Golden Ratio), as marked in Fig. 4(b) where 30 data points are included with error bars (12 points from natural samaras and 18 points from artificial samaras). In addition, selected data sets from previous studies [5,28,29] are also included, showing the consistent result (Table III [23]). The establishment of equilibrium, i.e., $\rho v^2 / (2\Delta) \approx 1.618$, in stable autorotation (*Stage III*) is associated with constant descent velocity (v), rotational speed (ω), pitch angle (θ), and cone angle (β). Each of these stable parameters requires the equilibrium of forces and moments.

Specifically, this analysis, therefore, reveals the intrinsic descent characteristic of samaras since all specimens follow the similar behavior in terms of free falling, transient positioning, and stable autorotation.

A summary of the samara's descent dynamics in the free falling (I), transient positioning (II) and stable autorotation (III) stages is provided based on the qualitative assessment of the high-speed images shown in Fig. 1. Upon releasing, the rotation of a samara appears to be initiated by its leading-edge weight, setting a negative (nose-down) pitch angle, which tends to incline the lift vector forwards to generate an unbalanced starting torque and angular acceleration in the free falling (I) and transient positioning stages (II). The angular velocity of the wing increases until the tangential components of the lift and drag forces (which contribute separately to wing driving and retarding torque) become balanced and constant rotational speed is established in the stable autorotation (III) stage. Simultaneously, with the increasing angular velocity, larger centripetal forces act on the mass elements that cause the samara to effectively open during the transient positioning stage and expose its lifting surface as shown in Fig. 1, thus enabling the samara to arrest the rate of its decent in comparison to the free-falling stage. A steady rotational rate is established in the stable autorotation stage (III) as seen by the constant pitch distance and repeating angular position of the samara between successive high-speed frames in Fig. 1. Therefore, the stable cone angle is dependent upon the generated lift and drag torques and the rotational speed. A stable descent velocity is realized by the samara when the combined upwards components of its lift and drag forces eventually find equilibrium with its downwards weight.

IV. CONCLUSION

The descent velocity (expressed in the form of dynamic pressure) of a stably autorotating single-winged body is determined by disc loading, regardless of its detailed wing shape, wing size and total mass, so long as its asymmetric mass distribution sustains the stable autorotation. In this way, the descent velocity of a given natural samara (or an artificial samara satisfying asymmetric mass distribution), can be readily estimated using premeasured disc loading via Eq. (1) ($1/C_L \sim 1.618$) or, reciprocally, the collective lift coefficient is about 0.618, which agrees with the data in previous studies, at least, for the particular types of samaras considered [28,29].

ACKNOWLEDGMENTS

This work was supported by the National Natural Science Foundation of China (11972185 and 12032010), the 111 Program (BP2018012), China, and the One-Belt-One-Road Innovative Talent Exchange Programme for Foreign Experts (DL20200010006), China.

- [1] E. J. Lee and S. J. Lee, Effect of initial attitude on autorotation flight of maple samaras (*Acer Palmatum*), *J. Mech. Sci. Technol* **30**, 741 (2016).
- [2] M. H. Sohn, H. S. Yoo, and J. G. Kwak, Numerical simulations of the autorotative flight of the real and artificial maple seeds, in *15th International Conference on Fluid Control, Measurements and Visualization* (University of Naples Federico II, Naples, 2019).
- [3] M. Y. Zakaria, C. R. dos Santos, A. Dayhoum, F. D. Marques, and M. R. Hajj, Modeling and prediction of aerodynamic characteristics of free fall rotating wing based on experiments, in *IOP Conference Series: Materials Science and Engineering* (IOP publishing, Cairo, 2019).
- [4] K. Varshney, S. Chang, and Z. J. Wang, The kinematics of falling maple seeds and the initial transition to a helical motion, *Nonlinearity* **25**, C1 (2011).
- [5] D. S. Green, The terminal velocity and dispersal of spinning samaras, *Am. J. Bot.* **67**, 1218 (1980).
- [6] C. K. Augspurger, Morphology and dispersal potential of wind-dispersed diaspores of neotropical trees, *Am. J. Bot.* **73**, 353 (1986).
- [7] D. F. Greene and E. A. Johnson, The aerodynamics of plumed seeds, *Funct. Ecol.* **4**, 117 (1990).
- [8] D. F. Greene and E. A. Johnson, Can the variation in samara mass and terminal velocity on an individual plant affect the distribution of dispersal distances? *Am. Nat.* **139**, 825 (1992).
- [9] D. F. Greene and E. A. Johnson, Seed mass and dispersal capacity in wind-dispersed diaspores, *Oikos* **67**, 69 (1993).
- [10] R. Nathan, G. G. Katul, H. S. Horn, S. M. Thomas, R. Oren, R. Avissar, S. W. Pacala, and S. A. Levin, Mechanisms of long-distance dispersal of seeds by wind, *Nature (London)* **418**, 409 (2002).
- [11] S. K. H. Win, C. H. Tan, D. S. B. Shaiful, J. E. Low, G. S. Soh, and S. Foong, The effects of chordwise wing optimization of single-winged samara in autorotation, in *2017 IEEE International Conference on Advanced Intelligent Mechatronics* (IEEE, Munich, 2017).
- [12] K. Fregene and C. L. Bolden, Dynamics and control of a biomimetic single-wing nano air vehicle, in *Proceedings of the 2010 American Control Conference*, Baltimore (IEEE, Baltimore, MD, 2010).
- [13] E. R. Ulrich, D. J. Pines, and J. S. Humbert, From falling to flying: The path to powered flight of a robotic samara nano air vehicle, *Bioinspir. Biomim.* **5**, 045009 (2010).
- [14] S. Thomas, D. Ho, A. Kerroux, L. Lixi, N. Rackham, and S. Rosenfeld, Concept and design of a biomimetic single-wing MAV, *Int. J. Eng.* **2**, 16 (2014).
- [15] S. K. H. Win, L. S. T. Win, D. Sufiyan, G. S. Soh, and S. Foong, Dynamics and control of a collaborative and separating descent of samara autorotating wings, *IEEE Robot. Autom. Lett.* **4**, 3067 (2019).
- [16] B. H. Kim *et al.*, Three-dimensional electronic microfliers inspired by wind-dispersed seeds, *Nature (London)* **597**, 503 (2021).
- [17] P. Pounds and S. Singh, Samara: biologically inspired self-deploying sensor networks, *IEEE Potentials* **34**, 10 (2015).
- [18] D. Lentink, W. B. Dickson, J. L. Van Leeuwen, and M. H. Dickinson, Leading-edge vortices elevate lift of autorotating plant seeds, *Science* **324**, 1438 (2009).
- [19] E. Salcedo, C. Treviño, R. O. Vargas, and L. Martínez-Suástegui, Stereoscopic particle image velocimetry measurements of the three-dimensional flow field of a descending autorotating mahogany seed (*Swietenia Macrophylla*), *J. Exp. Biol.* **216**, 2017 (2013).
- [20] S. J. Lee, E. J. Lee, and M. H. Sohn, Mechanism of autorotation flight of maple samaras (*Acer Palmatum*), *Exp. Fluids.* **55**, 1718 (2014).
- [21] D. Seter and A. Rosen, Study of the vertical autorotation of a single winged samara, *Biol. Rev.* **67**, 175 (1992).
- [22] D. Seter and A. Rosen, Stability of the vertical autorotation of a single-winged samara, *Appl. Mech.* **59**, 1000 (1992).
- [23] See Supplemental Material at <http://link.aps.org/supplemental/10.1103/PhysRevE.106.014405> for further details and additional supporting data.
- [24] D. C. Collis and M. J. Williams, Two-dimensional convection from heated wires at low Reynolds numbers, *J Fluid. Mech.* **6**, 357 (1959).
- [25] E. Kulunk, Aerodynamics of wind turbines. IntechOpen <https://www.intechopen.com/chapters/16241> (2011).
- [26] R. Å. Norberg, Autorotation, self-stability, and structure of single-winged fruits and seeds (samaras) with comparative remarks on animal flight, *Biol. Rev.* **48**, 561 (1973).
- [27] A. Rosen and D. Seter, Vertical autorotation of a single-winged samara, *Appl. Mech.* **58**, 1064 (1991).
- [28] A. Azuma and K. Yasuda, Flight performance of rotary seeds, *J. Theor. Biol.* **138**, 23 (1989).
- [29] S. Minami and A. Azuma, Various flying modes of wind-dispersal seeds, *J. Theor. Biol.* **225**, 1 (2003).